



HAL
open science

Prediction of the Synthesis of Spiro Derivatives by Double Intramolecular Aromatic Electrophilic Substitution Using Reactivity Indices

Clément Dalinot, Victorien Jeux, Lionel Sanguinet, Thomas Cauchy, Magali Allain, Yohann Morille, Valérie Bonnin, Philippe Leriche

► **To cite this version:**

Clément Dalinot, Victorien Jeux, Lionel Sanguinet, Thomas Cauchy, Magali Allain, et al.. Prediction of the Synthesis of Spiro Derivatives by Double Intramolecular Aromatic Electrophilic Substitution Using Reactivity Indices. ACS Omega, 2019, 4 (3), pp.4571-4583. 10.1021/acsomega.8b03368 . hal-02467135

HAL Id: hal-02467135

<https://hal.science/hal-02467135>

Submitted on 8 Jan 2024

HAL is a multi-disciplinary open access archive for the deposit and dissemination of scientific research documents, whether they are published or not. The documents may come from teaching and research institutions in France or abroad, or from public or private research centers.

L'archive ouverte pluridisciplinaire **HAL**, est destinée au dépôt et à la diffusion de documents scientifiques de niveau recherche, publiés ou non, émanant des établissements d'enseignement et de recherche français ou étrangers, des laboratoires publics ou privés.

Prediction of the Synthesis of Spiro Derivatives by Double Intramolecular Aromatic Electrophilic Substitution Using Reactivity Indices

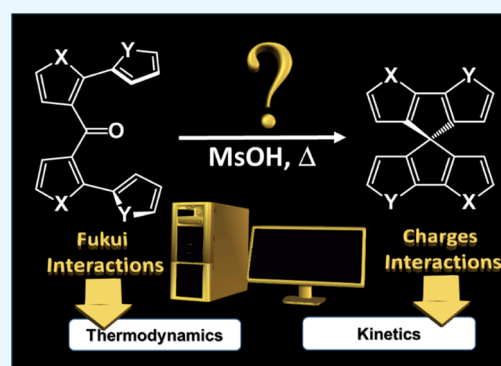
Clément Dalinot, Victorien Jeux, Lionel Sanguinet,*¹ Thomas Cauchy,² Magali Allain, Yohann Morille, Valérie Bonnin, and Philippe Leriche*

Laboratoire MOLTECH-Anjou, Université d'Angers, CNRS-UMR 6200, 2 Boulevard Lavoisier, 49045 Angers Cedex, France

Supporting Information

ABSTRACT: The synthesis of heterocyclic spirobifluorene (SBF) analogs generally requires long and complicated synthetic pathways. Despite this synthetic effort, such structural modification allows the (opto)electronic properties of this remarkable three-dimensional node to be tuned especially for molecular electronic applications. For this reason, the development of a simple, robust, and efficient synthetic methodology to introduce various heterocycles in place of classical phenyl rings in the spirofluorene motif is highly and timely desirable. In this context, we describe herein our efforts to develop a straightforward and efficient synthesis leading to replacement of 2 phenyl rings by various heterocycles in spiro compounds from 2,2'-dibromobenzophenone. As the same procedure to form fully heterocyclic compounds failed, an original theoretical approach based mainly on the uncommon Fukui dual function was developed in order to determine clearly the limitation of this strategy and provide an efficient predictive tool.

Indeed, such calculation allows prediction of the thermodynamic and kinetic aspects of the synthesis of spiro derivatives using a double aromatic electrophilic substitution. If this procedure reproduces well our experimental results focused on (heterocyclic) SBF compounds, it can be certainly adapted and generalized to other intramolecular substitutions.



INTRODUCTION

If many organic molecules incorporated as materials in organic electronics can be considered as one-dimensional π -conjugated systems, the elaboration of two-dimensional and even three-dimensional (3D) architectures represents a manner to modulate the degree of intra- and intermolecular interactions in materials.¹ Among the numerous examples of 3D structures reported,² the spirobifluorene (SBF)-based molecules appear as promising derivatives for organic electronics as they can present two perpendicular π -conjugated systems exhibiting identical or complementary properties. On one hand, the multiplication of π -conjugated systems may allow high mobilities³ and on the other hand, the presence of bulky groups associated with the 3D node can in contrary favor electroluminescence.⁴ In the same manner as dye-sensitized solar cell devices, several examples of SBF-based molecular or polymeric systems have been recently incorporated in organic solar cells (OSCs).⁵ In such devices, these systems allow higher photoconversion efficiencies than their fluorene analogues. Indeed, the spiro node seems to favor intermolecular interactions in the solid states associated with facilitated device fabrication because of an enhancement of the solubility.^{4b} In the organic photovoltaic field, the replacement of the phenyl moieties by heterocyclic units could be considered as a general trend to improve the performances

of the corresponding materials.⁶ Within this context, the chemical modification of the fluorene core, a promising arene candidate for OPV due to its rigidity, planarity, and stability toward photodegradation and thermal oxidation,⁷ has received considerable attention.⁸ The first approach consists of the replacement of the sp^3 bridging carbon by nitrogen (NR) or silicon (SiR_2) and has led to carbazole⁹ or silafluorene¹⁰ derivatives,^{7,11} as active materials in OSC. The second trend involves the replacement of phenyl cycles by thiophene rings thanks to advances in organic synthesis. This strategy led, for example, to the elaboration of several indacenodithiophene small molecules¹² and polymers presenting higher performances than the corresponding fluorene derivatives.¹³

All these results convinced us that incorporating, in molecular or polymeric systems designed for optoelectronics, a new generation of heterocyclic analogues of SBF should be interesting. If the preparation of thiophenic analogues of SBF is known for years, only few and recent examples of devices based on these compounds are reported, certainly because of synthesis issues. In fact, almost all described syntheses follow the main synthetic strategy used by Clarkson and Gomberg in

Received: December 1, 2018

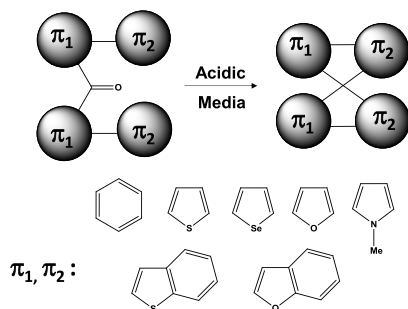
Accepted: February 19, 2019

Published: March 1, 2019

1930 to prepare 9,9'-spirobifluorene.¹⁴ This one implies in the first step a nucleophilic attack of a bicyclic compound onto a fluorenone analogue followed in the second step by an intramolecular cyclization in acidic conditions. This strategy successively applied by Sinnige,¹⁵ Bäuerle,¹⁶ and Kobayashi¹⁷ appears complex to optimize in the case of thiophenic derivatives because of the high reactivity of their terminal positions. Indeed, Bäuerle indicates that during the final cyclization step, the reaction conducts to the desired compounds (in low-moderate yields) but also to a mixture of oligomeric species resulting from intermolecular reactions. By involving suitable consecutive protected and unprotected steps of incriminated terminal positions, several compounds have been synthesized by the teams of Wong¹⁸ and Fungo.¹⁹ Moreover, the prefunctionalization of terminal positions may also in some cases partially avoid the unprotected step.²⁰ Nevertheless, in all these cases, the number of synthetic steps and overall yields may constitute an obstacle to the development of further devices.

More recently, Chiang et al. have suggested the second approach fulfilled for the preparation of disubstituted SBF derivatives²¹ such as the useful 2,2'-dibromo-9,9'-spirobifluorene.²² In this case, the treatment in acidic conditions of bis-biphenyl methanone by methane sulfonic acid (MsOH) leads in one step to the desired compound in good yields because of a double intramolecular electrophilic aromatic substitution (EAS) reaction (Scheme 1). If the first synthetic methodology

Scheme 1. Targeted SBF Derivatives by Double Intramolecular EAS Cyclization



developed by Clarkson and Gomberg was largely investigated for the preparation of heterocyclic analogues of SBF, this second one was surprisingly not explored. In this context, we report in this publication our efforts to prepare bi-heterocyclic analogues of SBF based on a double intramolecular EAS cyclization and then to generalize this methodology to tetra-heterocyclic compounds. For this reason, we have prepared two series of ketones substituted by bisaromatic systems including one or two heterocyclic motifs and carried out their acidic treatment with MsOH. If we have successfully obtained the targeted bi-heterocyclic spiro derivatives in most cases, our attempts to prepare full thiophenic SBF analogues by this methodology were ineffective.

In order to rationale these results and to provide a predictive tool, we conducted an original theoretical study of charges and orbital interaction factors driving this reaction. In fact, it is commonly admitted that EAS reactions are in their large majority under frontier orbital control.²³ Indeed, it was one of the first mechanisms described by Fukui et al. to stress the role of the frontier orbitals.²⁴ Nevertheless, in the present case, the involved ketonic species bear two identical and almost

independent conjugated systems. As a consequence, the frontier molecular orbitals (FMO) may be nearly degenerated and a rationale based only on FMO interactions could be misleading. Furthermore, charge interactions could also play a role as cationic reactive species resulting from the protonation of the ketone. Therefore, the rationale has been based on the calculated local electrophilicities, nucleophilicities, and hardness. Such concepts rationalized by Parr and Weitao using the density functional theory (DFT) can be considered nowadays as major reactivity indicators.²⁵ In this study, they are the key points to interpret the experimental observations and provide a projection on the possibilities of double EAS reaction concerning the various SBF analog preparations. More importantly, they represent the fundamentals of a prediction tool to fix the limitations of this synthetic methodology.

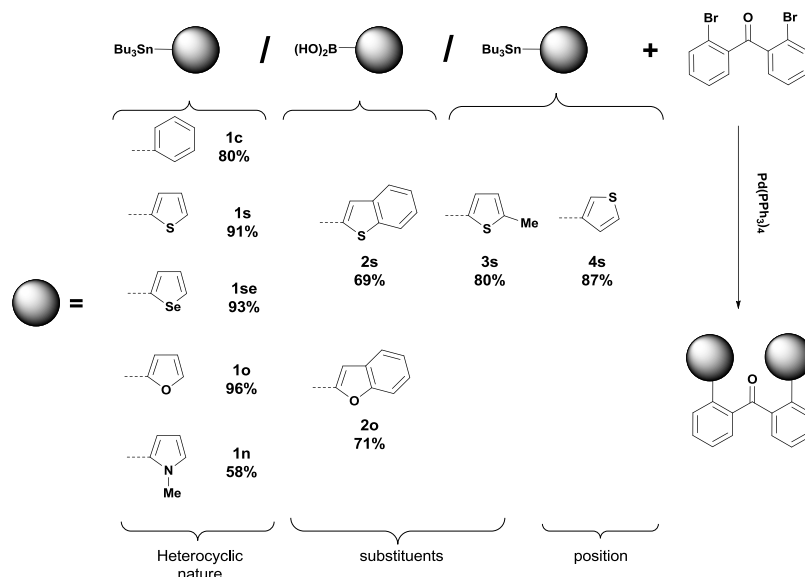
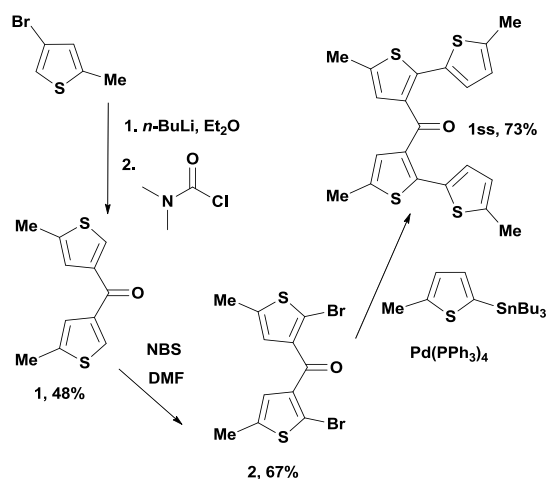
RESULTS AND DISCUSSION

Synthesis. In order to overview the possibilities to prepare heterocyclic SBF analogs by a double EAS, we have synthesized several bis-aryl ketones including a large variety of heterocycles. In this purpose, the commercially available 2,2'-dibromobenzophenone allows a straightforward synthesis of targets in one step by Stille or Suzuki coupling with the corresponding stannylated or boronic ester heterocycles. Following this procedure, 9 different ketones were prepared in yields oscillating between 58 and 93% spanning the incorporation of thiophenes (**1s**, **3s**, **4s**), benzothiophene (**2s**), furan (**1o**), benzofuran (**2o**), pyrrole (**1n**), or selenophene (**1se**) with various substitutions or position isomerisms (Scheme 2).

Pushing further the substitution of phenyl rings by heterocyclic ones requires in the first place the preparation of the corresponding heterocyclic analogues of 2,2'-dibromobenzophenone. Amongst the large number of possibilities, we voluntarily limited our study to full thiophenic analogs of SBF in reference to the preparation already described by Fungo (11 steps with an overall yield of 13%).¹⁹ In addition, the preparation of di-thiophen-3-yl-methanone by various procedures is well documented.²⁶ In this context, we targeted bis(2-bromo-5-methylthiophen-3-yl)methanone (**2**), as its terminal methyl groups are susceptible to avoid oligomerization resulting from intermolecular reaction during cyclization (vide infra). Completed by Stille coupling, the targeted bis(5,5'-dimethyl-[2,2'-bithiophen]-3-yl)methanone (**1ss**) was easily obtained with an overall yield of 23% in 3 steps from commercial 5-methyl-3-bromothiophene as described in Scheme 3.

The conversion of the prepared bis-aryl ketone derivatives into their corresponding spiro compounds requires strong acidic conditions first to increase the electrophile character of the central carbon and second to facilitate the dehydration of the intermediate carbinol.²⁷ For these reasons, we have adapted here the conditions developed by Chen et al. consisting of treating the corresponding ketone by methanesulfonic acid.²² We have used more diluted conditions ($C = 1.5 \times 10^{-3} \text{ mol}\cdot\text{L}^{-1}$) to limit harmful intermolecular reactions observed by Bäuerle when heterocycle terminal positions are unsubstituted.¹⁶ In all cases, this acidic treatment of the methanone derivatives at room temperature rapidly induces a strong reddish coloration, probably imputable to the protonation of the ketone. However, the observation of the intramolecular cyclization leading to the formation of the

Scheme 2. Syntheses of the Nine Targeted Ketones from 2,2'-Dibromobenzophenone by Stille or Suzuki Coupling

Scheme 3. Preparation of Bis(5,5'-dimethyl-[2,2'-bithiophen]-3-yl)methanone (**1ss**)

corresponding spiro compound was not observed every time (Table 1).


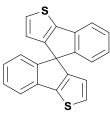
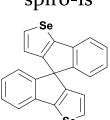
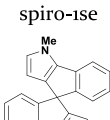
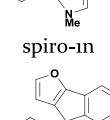
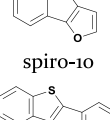
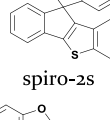
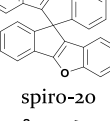
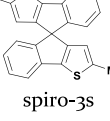
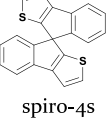
As shown in Table 1, the efficiency of the formation of the spiro derivative is strongly affected by the nature of the π -conjugated system borne by the ketone. In agreement with described preparation of 2,2'-dibromospirobifluorene by Cheng et al.,^{21b} the cyclization of ketone **1c** needs heating of the reaction mixture (Table 1, entry 1). After 12 h at 120 °C, unsubstituted SBF is isolated in 71% yield or in 57% for the two steps. On the opposite, the insertion of a more nucleophilic heterocycle than the phenyl ring such as a nude thiophene (**1s**, **3s**, **4s**), pyrrole (**1n**), or selenophene (**1se**) allows the obtainment of the targeted spiro compounds directly at room temperature in good to moderate yields. Owing to its low stability in acidic media,²⁸ the insertion of a furan unit (**1o**) conducts only to the full degradation of the ketone. The replacement of the furan by a benzofuran motif known for its higher stability remained unsuccessful in the formation of the targeted spiro molecule as it also led to degradation products.

In order to decrease the quantity of nonvolatile, toxic, and expensive methanesulfonic acid, several tests were conducted from **1s**. Using a diluted solution of sulfonic acid in chloroform or pentane still allows the observation of the targeted spiro derivative but the starting material remains preponderant even after one week. The opposite approach consisting of increasing compound concentration is also not satisfactory. It leads in all cases to a clear decrease of the yield associated with appearance of nonsoluble residues. These observations can be reasonably assigned to an increase of intermolecular cross-coupling as already observed in other conditions by Bäuerle and Mitschke.¹⁶ As mentioned above, suitable functionalization of the terminal position permits to limit side reactions and improves the spiro preparation efficiency. The first attempt with benzothiophene (**2s**) in place of thiophene moieties was undertaken and led to the desired molecule in 90% yield, the best registered here.

Moreover, using a methyl group to block the thiophene terminal position (**3s**) confirms this observation from a cheaper starting material. In this last case, it was possible to use up to 15 more concentrated solutions of **3s** and to continue to obtain the corresponding spiro **3s** in moderate good yield (47% with a concentration of $22 \times 10^{-3} \text{ mol}\cdot\text{L}^{-1}$). Thus, in this series, from nine ketones, if one excludes furan-based derivatives obviously nonstable in acidic conditions, spiro derivatives were isolated in reasonable yields when reactions were conducted in diluted conditions or from heteroaromatic compounds functionalized in their terminal position.

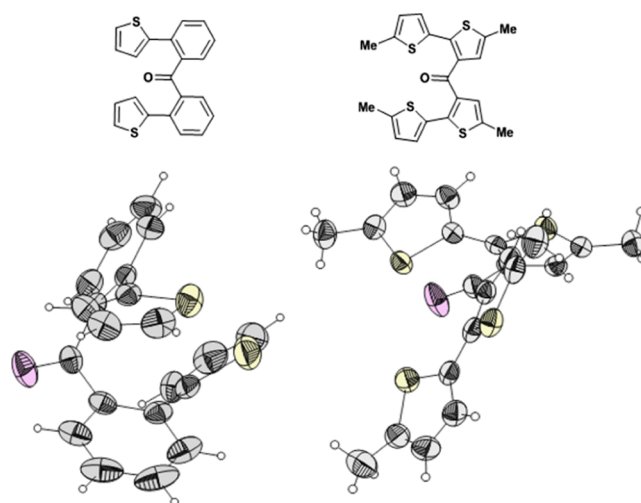
Based on these results, **1ss** which bears methyl groups on all the thiophenic terminal positions appears as an ideal platform to envision the preparation of a full heterocyclic analogue of SBF in the same conditions. First, experiments conducted at room temperature did not allow any reaction, and the starting material was isolated unchanged, despite observation of a reddish intense solution coloration assigned to the formation of the cationic intermediate (vide infra). By analogy with **1c** which cyclization requests a higher temperature, the solution was then heated at 40 °C. At this stage, a rapid degradation of **1ss** was noted without observation (even in MS) of the spiro target. In order to explain this reactivity difference between

Table 1. Substituent Effect on the Efficiency of Spiro-Derivative Preparation by Double EAS

Subs.	Conc. (mol.L ⁻¹)	Temp.	Product	Yield
1c	1.5 10 ⁻³	120°C	 spiro-1c	71%
1s	1.5 10 ⁻³	RT	 spiro-1s	73%
1se	1.5 10 ⁻³	RT	 spiro-1se	20%
1n	1.5 10 ⁻³	RT	 spiro-1n	74%
1o	1.5 10 ⁻³	RT	 spiro-1o	Not Observed
2s	1.5 10 ⁻³	RT	 spiro-2s	90%
2o	1.5 10 ⁻³	RT	 spiro-2o	Not Observed
3s	2.2 10 ⁻²	RT	 spiro-3s	47%
4s	1.5 10 ⁻³	RT	 spiro-4s	81%
1ss	1.5 10 ⁻³	RT	 spiro-1ss	Not Observed

ketonic compounds bearing a phenyl or a thiophenic ring, several series of analyses were conducted.

X-ray Analyses. The molecular structures of crystals obtained for **1c**, **1s**, **2s**, **4s**, **1se**, **1n**, **2s**, and **1ss** have been compared. X-ray structures of **1s** and **1ss**, both of which crystallize in an orthorhombic C2/c system, are briefly discussed and presented in [Figure 1](#) (other compounds

**Figure 1.** X-ray structures of compounds **1s** (left) and **1ss** (right).

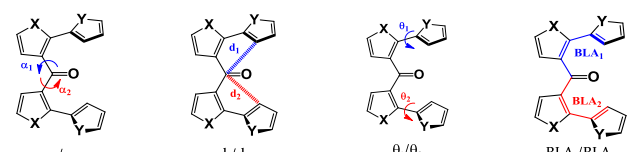
crystallographic data are provided in [Supporting Information](#)). When **1s** and **1ss** (as others) present encumbered 3D structures, few intermolecular interactions are observed within the obtained crystals.

Concerning intramolecular interactions, most compounds do not exhibit short distances between heterocyclic sulfur, oxygen, selenium atoms, and ketonic Oxygen. At the opposite, strong van der Waals intramolecular interactions are observed for compound **1ss**. Indeed, short distances (respectively, 2.72 and 2.70 Å) between its ketonic oxygen and lateral thiophenic sulfur atoms are observed in the solid state for this compound which does not cyclize under MsOH treatment.

Even if the study of X-ray structures does not indicate the conformational preference of compounds in solution, the latter can be considered as an interesting clue to understand reactivity differences. In order to highlight the similarities and differences between compounds several criteria were screened. Despite crystallization occurring in the centrosymmetric group for all compounds, it is important to note that no symmetric element is recovered in molecules. Thus, with two independent conjugated systems, the complete X-ray data analysis of each ketone should present two series of data including interaromatic angles (θ_1 , θ_2), dihedral angles between the carbonyl axis and grafted aromatic cycles (α_1 , α_2), bond length alternation (BLA) measurements (BLA₁, BLA₂), and distances between electrophilic and nucleophilic carbons (d_1 , d_2). All of these are reported in [Table 2](#).

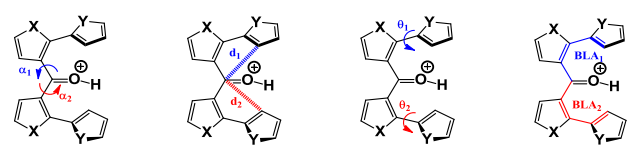
Interestingly, one can observe two main differences between the ketones undergoing an intramolecular cyclization and **1ss** which is not. First, **1ss** exhibits the longest distances between the carbonyl (electrophilic) and thiophenic carbon (nucleophilic) centers involved in the cyclization (4.54 and 4.56 Å for d_1 and d_2 , respectively). In fact, these distances are reduced by more than 1 Å for all other derivatives ranging from 3.15 to 3.25 Å ([Table 2](#)). Concerning compound **4s**, both 2- and 4-positions of the thiophene (referenced as C2 and C4, respectively, in [Tables 2](#) and [3](#)) can be considered as potential reactive locations for the intramolecular cyclization. Despite shorter distances between the electrophilic center and nucleophilic carbon C4, only the formation of **spiro-4s** resulting from the double cyclization in C2 positions is observed which can be reasonably explained by the well-known higher reactivity of the latter positions upon EAS reaction.²⁹

Table 2. Interaromatic Angles (θ_1, θ_2), Dihedral Angles between the Carbonyl Axis and Grafted Aromatic Cycles (α_1, α_2), Bond Length Alternation, and Distances (in Å) between Electrophilic and Nucleophilic Carbons (d_1, d_2) for All Ketone Derivatives Measured from Their X-ray Structure



Ketone	α_1/α_2	d_1/d_2	θ_1/θ_2	BLA ₁ /BLA ₂
1c	135.8/136.0	3.15/4.08	51.0/48.7	0.145/0.138
1s	44.7/42.5	3.22/3.27	51.3/52.8	0.136/0.137
2s	135.4/134.9	3.23/3.63	44.8/50.1	0.120/0.139
1se	46.4/42.7	3.23/3.27	51.5/52.8	0.144/0.127
1n	38.82/140.2	3.25/3.90	56.2/80.4	0.138/0.134
1ss	140.8/153.5	4.54/4.56	28.7/28.1	0.125/0.127
4s	136.4/135.6	C2: 3.85/4.14 C4: 3.18/3.18	43.5/46.7	0.135/0.142

Table 3. Interaromatic Angles (θ_1, θ_2), Dihedral Angles between the Carbonyl Axis and Grafted Aromatic Cycles (α_1, α_2), Bond Length Alternation, and Distances (in Å) between Electrophilic and Nucleophilic Carbons (d_1, d_2) for All Protonated Ketones Measured from the Corresponding Optimized Structure



Protonated Ketone	α_1/α_2	d_1/d_2	θ_1/θ_2	BLA ₁ /BLA ₂
1c	133.4/157.1	3.58/3.17	51.0/82.1	0.089/0.084
1s	42.9/33.0	3.24/3.21	44.5/43.1	0.076/0.060
2s	159.8/128.4	3.16/3.41	42.7/51.9	0.085/0.084
1se	32.2/42.0	3.21/3.23	45.2/42.8	0.076/0.059
1n	32.0/133.5	3.14/3.18	41.2/40.6	0.072/0.052
1ss	142.0/163.4	4.58/4.21	26.5/56.2	0.045/0.078
4s	137.5/152.0	C2: 4.25/4.24 C4: 3.26/3.20	44.6/45.0	0.080/0.066

Second, all ketones undergoing an intramolecular cyclization in acidic media to form the corresponding spiro derivative present a high dihedral angle (ranging from 38.7 to 80.4°) between vicinal heterocycles. In fact, only **1ss** exhibits two low angle values with 28.7° and 28.1° (Table 2). As a consequence, the less encumbered bithiophenic motif should conduct to an extension of the conjugation over both cycles. This observation is assessed by the measurement of BLA which is defined as the average of the difference in length between adjacent carbon-carbon bonds in a polyene chain. In this purpose, Table 2 gathers the BLA of the two considered conjugated skeletons on both sides of the carbonyl electrophilic motif (represented in red and blue) for all ketone derivatives. It is worth to note that, as expected, a lower BLA, that is, a better conjugation between the electron-rich and -deficient parts of the molecule is observed for **1ss**. However, solid-state structures of ketones cannot prefigure the behavior of their corresponding protonated forms in high polar and protic solution. These observations allow us to only presume that the electron densities of nucleophilic and electrophilic centers associated to their distance separation are the two main parameters which drive here the reactivity. In this context, if one excludes furan-based ketones (**1o** and **2o**) nonstable in acidic conditions, the lack of reactivity of **1ss** may be due to conjugation of high distance and predictable lower electron density on the nucleophilic centers due to a higher conjugation with the carbonyl motif.

Calculations. To stress such hypothesis, theoretical calculations have been carried out. As experimental evidences demonstrate the formation of a colorful cationic intermediate in all cases, the calculations were launched on the cationic form of the protonated ketone which can be considered as the reactive species. A conceptual DFT approach has been chosen (see Computational Details) as it offers interesting and efficient tools for this reactivity problem. The first computational step implies geometric optimizations starting from the X-ray diffraction positions of the ketone manually protonated.

Starting from optimized geometries, interaromatic angles (θ_1, θ_2), dihedral angles between the carbonyl axis and grafted aromatic cycles (α_1, α_2), BLA and distances between electrophilic and nucleophilic carbons (d_1, d_2) were determined for each derivative and gathered in Table 3. As we can see, calculated data collected on Table 3 for the protonated species are coherent with those measured on the corresponding ketone crystals (Table 2). It results that protonation and charge do not affect much the geometry, and similar trends are observed. A longer distance between electrophilic and nucleophilic centers is still observed for the protonated **1ss** (4.21 Å) in comparison with other compounds where it oscillates between 3.17 and 3.24 Å. Moreover, the calculated smaller interaromatic angle (θ_1 or θ_2) for **1ss** only attains 26.5° in contrast with others all of which present angles higher than 41.2°. This latter observation is in accordance with the lower BLA registered for **1ss** and indicates a global higher conjugation between electro- and nucleophilic parts of the

molecule and then a probable lower reactivity. However, the difference of reactivity and the necessity to heat the reaction mixture in some cases could not be rationalized only by these conformational variations.

As EASs are usually under frontier orbital control,³⁰ we looked at the highest occupied molecular orbital (HOMO) topology for the nucleophilic sites and at the lowest unoccupied molecular orbital (LUMO) topology for the electrophilic ones. The FMO plots are represented in Figure 2 for the **1c** and **1ss** cationic compounds (all other FMO plots

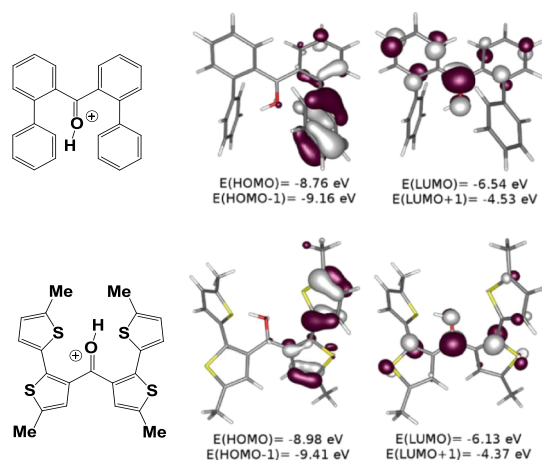


Figure 2. FMO plots (cutoff value was set to 20%) for the cations of **1c** above and **1ss** below.

are provided in Supporting Information). It is worth noting that the HOMO in all cases is essentially centered only on one of the two conjugated systems grafted on the ketone motif. It is a consequence of the asymmetry between the two arms because of the protonation of the carbonyl function. In addition, it can be noted that the HOMO of all compounds exhibits reasonable coefficients on the expected nucleophilic carbons. Nevertheless, they are not large and different enough to explain the reactivity differences. Concerning the HOMO – 1, they are the mirror images of the HOMO but centered on the other arm. Their energies are usually at least 0.3 eV below the corresponding HOMO levels, excepted for **4s** where the two levels are only separated by 0.06 eV. At the opposite, a stronger difference in energy (at least 2 eV) separates the LUMO and LUMO + 1 levels for all compounds.

Located on the carbon of the protonated carbonyl, main LUMO level contributions allow identification of the electrophilic center involved in EAS cyclization. All compounds present high LUMO coefficients on this part of their skeleton.

In order to rationale the reactivity of charged species (considered as hard reactants) involved in a reaction pathway, the electrostatic potential has generally to be investigated.³² Requiring important calculation resources,^{32b} the calculated molecular electrostatic potential maps on our protonated ketones do not provide satisfactory results. First, their encumbered and folded 3D structures do not facilitate the clear visualization of the electrostatic potential variation along the different sites. Second, the different protonated ketones see their positive charge delocalized on the whole molecule. The present intramolecular cyclization process involving two sites bearing a delocalized positive charge, the molecular electrostatic potential maps are then essentially positive. It only confirms the strong electrophilicity of the protonated carbonyl

carbon (vide infra). Nevertheless, they are not large and different enough to explain the reactivity differences. In this context, even if they are not expected to perform well in the case of charge-controlled reactions,³³ the Fukui functions were calculated to identify the different nucleophilic sites.

These functions are defined as the electron density differences (ρ) between the same molecule when one electron is gained ($N + 1$ electrons) or when an electron is lost ($N - 1$ electrons), without geometry modifications. As a consequence, two Fukui functions can be defined. First, the electrophilic Fukui function, f^+ , resulting from the addition of an electron [$\rho(N + 1) - \rho(N)$], shows the regions where electrophilicity is important. Therefore, if f^+ is similar to the square of the LUMO, the contribution of other orbitals and the electronic reorganization are negligible. Symmetrically, the nucleophilic Fukui function, f^- , is obtained by the electron density difference [$\rho(N) - \rho(N - 1)$] and should be compared to the square of the HOMO. The Fukui function plots are represented in Figure 3 for the **1c** and **1ss** cationic compounds

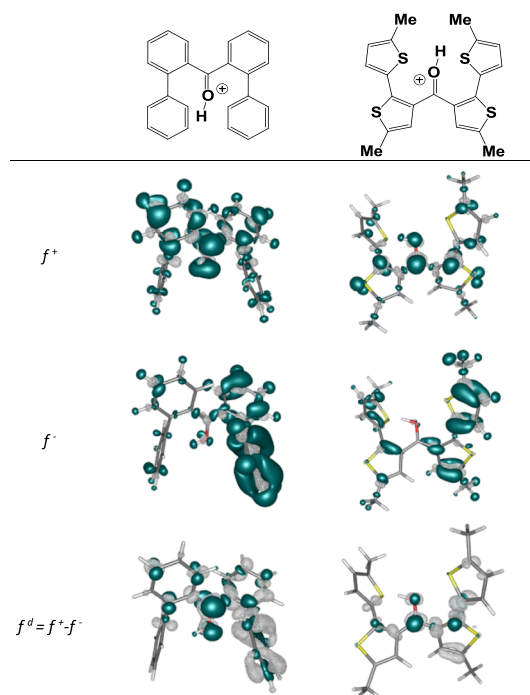


Figure 3. Representation of the electrophilic (f^+) and nucleophilic (f^-) Fukui function plots (cutoff value: 25%) for the cations of **1c** and **1ss** where the white hollow surfaces (negative Fukui functions) are due to the orbital relaxation but are not in this case qualitatively important³¹ and the corresponding dual descriptor ($f^d = f^+ - f^-$) plots (cutoff value: 25%) where the blue and white surfaces represent, respectively, the electrophilic and nucleophilic sites.

(see Supporting Information for all other protonated ketones). A clear likeness is observed for all compounds between the square of the FMOs and the Fukui functions, even for **4s** which presents an almost degenerated HOMO. One critical detail emerges from the FMO and Fukui function scrupulous observation. In fact, some carbon positions involved in the cyclization appear in both f^- and f^+ representations, especially in the case of **1ss**. It induces that a same position could present both an electrophilic and nucleophilic reactivity. As a consequence, the dual descriptor ($f^d = f^+ - f^-$) introduced by Morell et al.³⁴ seems to be a more convenient tool to

Table 4. Sum of the Coulomb Integral Using the Atomic Value (Called Condensed Values and Noted by the Alpha Letter) of Either the Dual Descriptors (C_{dual}) or the Charges (C_{charge}), Where r represents the Distance between the “Nucleophilic” and “Electrophilic” Carbons

	substrate						
	1c	1s	1se	1n	2s	4s	1ss
$C_{\text{dual}} = \sum \frac{f_{\alpha,\text{nucleophile}}^d f_{\alpha,\text{electrophile}}^d}{r_{\text{nucleophile-electrophile}}} \times 1000$	-5.7	-3.1	-2.9	-1.1	-3.2	-4.3	-0.3
$C_{\text{charge}} = \sum \frac{q_{\alpha,\text{nucleophile}} q_{\alpha,\text{electrophile}}}{r_{\text{nucleophile-electrophile}}} \times 1000$	+2.5	+0.01	+0.4	-2.7	+0.6	-1.4	+1.3
corresponding spiro formation yield (%)	71 ^a	73	20	74	90	81	0

apprehend an intramolecular reactivity problem as in our case. As this latter is based on both Fukui functions, it allows direct assessment of the local main reactivity in one picture.³⁴ The dual descriptors for compounds **1c** and **1ss** are plotted in Figure 3. The solid blue surfaces highlight the electrophilic sites, as the white hollow surfaces represent the nucleophilic ones. In this representation, the electrophilicity of the protonated ketone carbon is well confirmed for both compounds. At the opposite, a strong differentiation concerning the nucleophilic centers between **1ss** and other protonated ketones is clearly highlighted. In the case of ketones undergoing intramolecular cyclization, the involved aromatic positions exhibit a large positive contribution in dual descriptors as demonstrated by the large white hollow on the ortho position in the case of **1c** (Figure 3). Concerning **1ss**, the f^d plot reveals that the C3 thiophenic carbons potentially involved to form the corresponding spiro motif present almost negligible contributions. As a consequence, these positions are neither electrophilic nor nucleophilic, and then just inactive for intramolecular EAS reaction.

To prevent an abusive conclusion drawn on a picture depending on cutoff values, the condensed dual descriptor values associated with each atom were obtained through the Hirshfeld charge difference method (see Computational Details). Starting from this, the general reactivity indicator proposed by Anderson et al. can be used as it can describe both the charge and frontier orbital control of the chemical reactions.³⁵ Nonetheless, this latter depends on the quantity of transferred electrons between the nucleophile and the electrophile. In the case of an intramolecular reaction, this quantity is ill-defined. Hence, we focused on the main term relating the orbital interaction, described and named by Berkowitz, the coulomb integral between Fukui functions.³⁶ As a consequence, this integral was adapted to the condensed forms of the dual descriptor. The sum (C_{dual}) of all the interactions between the different nucleophile carbons with the electrophile ones were thus considered, and the calculated values are reported in Table 4 for all ketone derivatives. As the dual descriptor values are negative for electrophile sites and positive for nucleophile ones, the product is expected to be negative. As a consequence, a large negative value denotes a favorable thermodynamic stabilization. Owing to the less active nucleophilic sites, the **1ss** compound presents an overall sum (-0.3) up to ten times weaker than the other compounds what clearly rationalizes its noncyclization.

As the Fukui functions and the FMO control, the dual descriptor is mainly associated to the thermodynamic control. The dual descriptor cannot, then, fully reflect the changes observed in the yields of spiro compound formation.

Obviously, the reaction yield results from multiple steps of synthesis and the purification process and cannot be precisely predicted with just a rationale based on the reactants. A full prediction of the whole mechanism is then out of the scope of this article. In order to get some clues on the observed yield differences and required thermal activation for spiro-derivative preparation, the interactions between the charges have been studied to include long-range effects³⁷ (see Table 1). Indeed, the protonation of the ketone seems to conduct to a strong enhancement of its electrophile character; however, on the other hand, the generated charge will be delocalized on the conjugated arm and could lead to calculated small positive charges on the expected nucleophile heteroaromatic positions reducing their reactivity. In the most favorable cases, they will induce a suitable orientation of the system and then promote the first intramolecular EAS reaction. On the contrary, a thermal activation of the reaction mixture will be required to overcome an additional reaction barrier induced by unfavorable small repulsion resulting from charge interactions. Because the molecular electrostatic potential maps are not clear, we have transposed the formula used to determine C_{dual} to the atomic charges of the protonated ketones in order to reflect the charge interactions.

Therefore, these pseudo-Coulomb interaction values, C_{charge} were calculated for all protonated ketones and reported in Table 4 revealing a rationale. Indeed, as for C_{dual} , a large C_{charge} negative value indicates a favorable interaction. Therefore, calculations conclude to an overall unfavorable charge repartition in some cases translated by a positive value of C_{charge} such as compound **1c**.

Effectively, the **1c** system has to overcome an important electrostatic repulsion ($C_{\text{charge}} = +2.5$) to undergo the cyclization process largely thermodynamically favored ($C_{\text{dual}} = -5.7$). Starting from this, the formation of spiro-**1c** only at high temperature is well explained by both antagonist effects. At the light of these results, the poor yield observed for spiro-**1se** can be reasonably rationalized by an unfavorable kinetic competition between the cyclization process and possible side reactions such as intermolecular cross-coupling. In this context, a thorough optimization of the thermal and dilution conditions could permit to improve the efficiency of this thermodynamically feasible reaction ($C_{\text{dual}} = -2.9$). At the opposite, the obtainment following this methodology of the corresponding spiro derivative starting from **1ss** seems compromised regarding disadvantageous charges and orbital interaction indicators.

CONCLUSIONS

We have prepared six new biheterocyclic SBF analogues following a simple synthesis methodology based on a double EAS reaction in only two steps with a global yield ranging from 20 to 70%. According to experimental observations, this synthetic pathway permits large structural modifications of classical SBF in order to tune its electronic properties with the substitution of two phenyl rings by various heterocycles. Despite our efforts, this synthesis approach remains not applicable to the preparation of the full thiophenic SBF.

In order to rationalize our results, we have set up a conceptual DFT approach. By performing geometric optimizations of the protonated ketones followed by the calculation of the Fukui dual descriptors, we have identified two key parameters allowing predicting their reactivity toward EAS reaction: the dual descriptors (C_{dual}) and the atomic charges (C_{charge}). The determination of these reactivity indicators allows evaluating the thermodynamic and kinetic aspects of the involved intramolecular EAS reaction. In this context, the required thermal activation, yield decrease, and reaction inefficiency experimentally observed are well correlated. To conclude, the original theoretical approach developed in this study can obviously serve as an efficient predictive tool for those who are interested in the design and the preparation of new spiro nodes by double intramolecular EAS. More generally, it could also pave the way to the development of a rationale concerning other intramolecular chemical processes where the classical frontier orbital approach does not fulfill researcher expectation.

MATERIALS AND METHODS

Commercially available (Aldrich, Alfa Aesar, and abcr) chemicals were used as received. The catalyst $\text{Pd}(\text{PPh}_3)_4$ was synthesized according to a literature reference and stored under an argon atmosphere in the fridge.³⁸ Diethylether (Et_2O) was freshly distilled from sodium each time prior to the reaction. Solvents (1,2-dimethoxyethane/water, 4:1) employed in Suzuki couplings were always degassed with argon prior to utilization. Organolithium reagent $n\text{BuLi}$ (1.6 M in hexanes) was purchased from ACROS (AcroSeal) and was regularly standardized using diphenylacetic acid. For flash chromatography, silica gel (Fluka, 60 Å pore size, 230–400 Å mesh) was used for all described compounds. NMR analysis was carried out using Bruker AVANCE 300 and Bruker AVANCE II 400 spectrometers in CDCl_3 at 25 °C. Chemical shifts are reported in ppm relative to the solvent (CDCl_3) residual value: $\delta = 7.26$ for ^1H NMR and $\delta = 77.16$ for ^{13}C NMR. Coupling constants are reported in hertz and rounded to the nearest 0.1 Hz. Mass spectra were acquired on a time-of-flight (TOF) mass spectrometer AccuTOF GCv by JEOL using an FD emitter (10 kV). Infrared spectra were recorded using a PerkinElmer Spectrum 100 spectrometer. Melting points were determined using Büchi melting point apparatus B-540. Cyclic voltammetry was performed in a three-electrode cell equipped with a platinum millielectrode, a platinum wire counter electrode and a silver wire used as a quasi-reference electrode. The voltammograms were recorded on a potentiostat/galvanostat (BioLogic-SP150) driven by EC-Lab software with positive feedback compensation. Based on repetitive measurements, absolute errors on potentials were estimated to be $\approx \pm 5$ mV. All the potentials reported were calibrated versus ferrocene/

ferrocenium oxidation potential (+0.405 V vs SCE or +0.425 V vs Ag/AgCl).

Synthesis Procedures. General Procedure for the Stille Coupling of 2,2'-Dibromobenzophenone. A mixture of 2,2'-dibromobenzophenone, an organotin compound (2.5 equiv), and $\text{Pd}(\text{PPh}_3)_4$ is dissolved in toluene. The solution is degassed for 30 min (Ar) and then is refluxed overnight under argon. After concentration, the residue is dissolved in CH_2Cl_2 and the organic phase is washed with water. After drying over MgSO_4 , the solvent is removed. The crude material is purified by column chromatography on silica gel using a mixture of pentane and methylene chloride (1/1) as the eluent to afford the desired compound.

Di([1,1'-biphenyl]-2-yl)methanone (1c). 2,2'-Dibromobenzophenone (500 mg, 1.47 mmol), phenyltributyltin (1.30 g, 3.53 mmol), $\text{Pd}(\text{PPh}_3)_4$ (169 mg, 10 mol %), and toluene (20 mL), (395 mg, 80%) are used. Monocrystals are obtained by crystallization in EtOH. X-ray structure: orthorhombic, $Pbca$. ^1H NMR (300 MHz, CDCl_3 , ppm): δ 7.41 (dd, $J = 7.7, 1.0, 2\text{H}$), 7.33 (td, $J = 7.5, 1.3$ Hz, 2H), 7.23–7.13 (m, 10H), 7.13–7.07 (m, 4H). IR (neat): 1671, 1248, 926, 747, 695 cm^{-1} . mp 165 °C. Physical data are in agreement with those reported in the literature.³⁹

Bis(2-(thiophen-2-yl)phenyl)methanone (1s). 2,2'-Dibromobenzophenone (600 mg, 1.76 mmol), 2-tributylstannylthiophene (1.4 mL, 4.4 mmol), $\text{Pd}(\text{PPh}_3)_4$ (100 mg, 5 mol %), and toluene (15 mL) are used; the product is obtained as a pale yellow solid (556 mg, 91%). Monocrystals are obtained by crystallization in EtOH. X-ray structure: monoclinic, $C2/c$. ^1H NMR (300 MHz, CDCl_3 , ppm): δ 7.41 (dd, 2H, $J = 7.5, 0.9$ Hz), 7.40–7.20 (m, 6H), 7.16 (dd, 2H, $J = 4.2, 2.1$ Hz), 6.85 (m, 4 H). ^{13}C NMR (125 MHz, CDCl_3 , ppm): δ 199.4, 141.4, 139.4, 133.9, 131.1, 130.6, 130.5, 128.1, 127.3, 127.0, 126.1. IR (neat): 1654, 1591, 1292, 927, 834, 764, 637, 498 cm^{-1} . mp 120 °C. HRMS (FAB): $[\text{M}^{+\bullet}]$ calcd 346.0481; found, 346.0471.

Bis(2-(selenophen-2-yl)phenyl)methanone (1se). 2,2'-Dibromobenzophenone (300 mg, 0.88 mmol), trimethyl-(selenophen-2-yl)stannane (570 mg, 1.94 mmol), $\text{Pd}(\text{PPh}_3)_4$ (200 mg, 20 mol %), and toluene (30 mL) are used; the product is obtained as a pale yellow solid (360 mg, 93%). Monocrystals are obtained by crystallization in EtOH. X-ray structure: orthorhombic, $C2/c$. ^1H NMR (300 MHz, CDCl_3 , ppm): δ 7.86 (dd, $J = 5.6, 1.1$ Hz, 2H), 7.38 (dd, $J = 7.5, 1.5$ Hz, 2H), 7.33 (dd, $J = 7.2, 1.5$ Hz, 2H), 7.29 (td, $J = 7.8, 1.5$ Hz, 2H), 7.21 (td, $J = 7.2, 1.6$ Hz, 2H), 7.08 (dd, $J = 5.6, 3.7$ Hz, 2H), 6.93 (dd, $J = 3.6, 1.0$ Hz, 2H). ^{13}C NMR (75 MHz, CDCl_3 , ppm): δ 199.8, 147.5, 139.1, 135.9, 132.1, 131.4, 130.6, 130.6, 130.5, 129.5, 127.3. IR (neat): 1654, 1290, 760, 684, 653, 442 cm^{-1} . mp 122 °C. MS (MALDI-TOF) $[\text{MH}^+]$: 441.1. HRMS (IE): $[\text{M}^{+\bullet}]$ calcd 441.9375; found, 441.9385.

Bis(2-(1-methyl-1H-pyrrol-2-yl)phenyl)methanone (1n). 2,2'-Dibromobenzophenone (450 mg, 1.32 mmol), 1-methyl-2-(tributylstannyl)-1H-pyrrole (1.08 g, 2.91 mmol); $\text{Pd}(\text{PPh}_3)_4$ (300 mg, 20 mol %), and toluene (40 mL) are used; the product is obtained as a pale yellow solid (260 mg, 58%). Monocrystals are obtained by crystallization in ethanol. X-ray structure: monoclinic, $P2_1/c$. ^1H NMR (300 MHz, CDCl_3 , ppm): δ 7.33 (td, $J = 7.4, 1.5$ Hz, 2H), 7.21 (td, $J = 7.5, 1.2$ Hz, 2H), 7.14 (m, 4H), 6.48 (dd, $J = 2.4, 1.9$ Hz, 2H), 5.96 (dd, $J = 3.5, 2.7$ Hz, 2H), 5.80 (dd, $J = 3.6, 1.8$ Hz, 2H), 3.19 (s, 6H). ^{13}C NMR (75 MHz, CDCl_3 , ppm): δ 201.0, 141.7, 131.8, 131.5, 131.2, 129.8, 128.3, 127.4, 122.4, 110.3,

107.8, 34.2. IR (neat): 1656, 1294, 931, 705 cm^{-1} . mp 104 °C. HRMS (FAB): calcd 340.1576; found, 340.1573.

Bis(2-(furan-2-yl)phenyl)methanone (1o). 2,2'-Dibromobenzophenone (500 mg, 1.47 mmol), tributyl(furan-2-yl)stannane (1.16 g, 3.24 mmol), Pd(PPh₃)₄ (169 mg, 10 mol %), and toluene (20 mL) are used; the product is obtained as a pale yellow solid (444 mg, 96%). Monocrystals are obtained by crystallization in EtOH. X-ray structure: orthorhombic, *Pna*2₁. ¹H NMR (300 MHz, CDCl₃, ppm): δ 7.59 (d, *J* = 7.2 Hz, 2H), 7.49–7.44 (m, 4H), 7.31–7.26 (m, 4H), 6.60 (d, *J* = 3.3 Hz, 2H), 6.33 (dd, *J* = 3.3, 1.8 Hz, 2H). ¹³C NMR (75 MHz, CDCl₃, ppm): δ 198.5, 152.4, 142.9, 137.4, 131.1, 130.4, 130.3, 128.5, 127.4, 111.6, 109.1. IR (neat): 1671, 1250, 1002, 927, 763, 733, 594 cm^{-1} . mp 70 °C. MS (MALDI-TOF) [*M*⁺]: 314.2. HRMS (FAB): [*M*⁺] calcd 314.0943; found, 314.10.

Bis(2-(5-methylthiophen-2-yl)phenyl)methanone (3s). 2,2'-Dibromobenzophenone (0.514 g, 1.51 mmol), tributyl(5-methylthiophen-2-yl)stannane (1.29 g, 3.33 mmol), Pd(PPh₃)₄ (174 mg, 10 mol %), and toluene (30 mL) are used; the product is obtained as a pale yellow solid (410 mg, 72%). ¹H NMR (300 MHz, CDCl₃, ppm): δ 7.38–7.21 (m, 8H), 6.66 (d, *J* = 2.7 Hz, 2H), 6.51 (s, 2H), 2.39 (s, 6H). ¹³C NMR (75 MHz, CDCl₃, ppm): δ 199.5, 140.8, 139.4, 139.3, 134.5, 131.1, 130.6, 130.5, 128.1, 127.0, 125.5, 15.3. IR (neat): 1715, 1265, 760 cm^{-1} . mp 160 °C. MALDI-TOF: 374.1. HRMS (FAB⁺): calcd 374.0799; found, 374.0801.

Bis(2-(thiophen-3-yl)phenyl)methanone (4s). 2,2'-Dibromobenzophenone (0.3 g, 0.88 mmol), 3-tributylstannylthiophene (0.82 g, 2.2 mmol), Pd(PPh₃)₄ (80 mg, 8 mol %), and toluene (10 mL) are used; the product is obtained as a white solid (264 mg, 87%). Monocrystals are obtained by slow evaporation of a solution of methylene chloride/pentane (1/1). X-ray structure: monoclinic, *C2/c*. ¹H NMR (300 MHz, CDCl₃, ppm): δ 7.43 (dd, 2H, *J* = 8.1, 1.5 Hz), 7.36 (td, 2H, *J* = 7.5, 1.5 Hz), 7.24 (m, 4H), 7.12 (dd, 2H, *J* = 4.8 Hz, *J* = 3 Hz), 7.02 (dd, 2H, *J* = 3, 1.2 Hz), 6.87 (dd, 2H, *J* = 5.1, 1.2 Hz). ¹³C NMR (75 MHz, CDCl₃, ppm): δ 199.9, 140.8, 139, 136.2, 130.8, 130.3, 130.2, 128.7, 126.9, 124.9, 123.5. HRMS (FAB): calcd 346.0481; found, 346.0492.

General Procedure for the Suzuki Coupling of 2,2'-Dibromobenzophenone. To a stirred suspension of 2,2'-dibromobenzophenone in dioxane was added a mixture of Na₂CO₃ and the corresponding boronic acid compound in water. The mixture was degassed for 30 min with argon prior addition of Pd(PPh₃)₄, and then, the reaction mixture was heated to 110 °C overnight. After cooling to room temperature, the organic phases were extracted with CH₂Cl₂, dried over MgSO₄, and the solvent was removed under vacuum. The crude product was purified by chromatography on silica gel using a mixture of pentane/methylene chloride (1/1) to afford the desired compound.

Bis(2-(benzofuran-2-yl)phenyl)methanone (2o). 2,2'-Dibromobenzophenone (0.5 g, 1.47 mmol), dioxane (60 mL), Na₂CO₃ (1.55 g, 14.7 mmol), and benzo[*b*]furan-2-ylboronic acid (571 mg, 3.53 mmol) are used; the product is obtained as a pale yellow solid (430 mg, 71%). Monocrystals are obtained by crystallization in ethanol. X-ray structure: tetragonal, *P4*₂2₁. ¹H NMR (300 MHz, CDCl₃, ppm): δ 7.62 (d, *J* = 7.7 Hz, 2H), 7.57 (d, *J* = 7.6 Hz, 2H), 7.48 (dd, *J* = 6.3, 2.3 Hz, 2H), 7.38 (dd, *J* = 10.7, 4.4 Hz, 2H), 7.31–7.12 (m, 9H), 6.94 (s, 2H). ¹³C NMR (75 MHz, CDCl₃, ppm): δ 198.1, 155.0, 154.4, 137.9, 131.0, 130.4, 130.0, 129.1, 128.6, 128.3, 124.4, 122.8, 121.1, 111.2, 105.7. IR (neat): 1689, 1444, 1247, 929,

745 cm^{-1} . mp 110 °C. HRMS: calcd 414.1256; found, 414.1251.

Bis(2-(benzo[*b*]thiophen-2-yl)phenyl) Methanone (2s). 2,2'-Dibromobenzophenone (0.5 g, 1.47 mmol), dioxane (60 mL), Na₂CO₃ (1.55 g, 14.7 mmol), and benzo[*b*]thiophen-2-ylboronic acid (628 mg, 3.53 mmol) are used; the product is obtained as a pale yellow solid (450 mg, 69%). Monocrystals are obtained by crystallization in EtOH. X-ray structure: orthorhombic, *Pbca*. ¹H NMR (300 MHz, CDCl₃, ppm): δ 7.75–7.70 (dd, *J* = 8.4, 1.5 Hz, 2H), 7.65 (dd, *J* = 6.5, 2.1 Hz, 2H), 7.44 (dd, *J* = 7.7, 0.9 Hz, 2H), 7.35 (dd, *J* = 7.7, 0.9 Hz, 2H), 7.33–7.27 (m, 6H), 7.14 (td, *J* = 7.6, 1.4 Hz, 2H), 7.05 (s, 2H). ¹³C NMR (75 MHz, CDCl₃, ppm): δ 199.2, 141.8, 140.5, 139.9, 139.6, 134.0, 131.2, 130.7, 130.6, 127.7, 125.0, 124.4, 124.3, 123.7, 121.9. IR (neat): 1667, 1428, 1243, 940, 916, 753, 725, 438 cm^{-1} . mp 162 °C. MALDI-TOF: 446.1. HRMS (FAB⁺): calcd 446.0799; found, 446.0803.

Bis(5-methylthiophen-3-yl)methanone (1). To a solution of 4-bromo-2-methylthiophene (3.16 mL, 28.24 mmol) in 50 mL of diethyl ether at –78 °C under an Ar atmosphere, *n*-BuLi (2.5 M in hexanes, 12.43 mL, 31.06 mmol) is dropwise added. After 15 min of stirring at the same temperature, dimethylcarbamic chloride (1.43 mL, 15.53 mmol) is added and the reaction mixture is stirred at –78 °C for 1 h before allowing it to warm to room temperature. The solution is hydrolyzed with water and extracted with diethyl ether, and the combined organic phases are dried over MgSO₄. The crude product is purified by column chromatography on silica gel, using a mixture of methylene chloride/cyclohexane (1/1) as the eluent to afford a pale yellow solid (1.5 g, 48%). ¹H NMR (300 MHz, CDCl₃, ppm): δ 7.70 (d, *J* = 1.4 Hz, 2H), 7.20 (m, 2H), 2.47 (d, *J* = 1.1 Hz, 6H). ¹³C NMR (75 MHz, CDCl₃, ppm): δ 183.2, 141.8, 140.7, 130.8, 126.0, 15.1. IR (neat): 1611, 1436, 1395, 1230, 850, 725, 474 cm^{-1} . mp 118 °C. HRMS (MALDI-TOF): [*M*⁺] calcd 222.0173; found, 222.0168.

Bis(2-bromo-5-methylthiophen-3-yl)methanone (2). In the dark, to a solution of bis(5-methylthiophen-3-yl)methanone (700 mg, 3.15 mmol) in dimethylformamide (DMF) (20 mL) is added a solution of NBS (1.23 g, 6.93 mmol) in DMF (20 mL). The resulting mixture is stirred for 12 h at room temperature and poured into water; the mixture is extracted with methylene chloride. The organic phase is washed with a solution of ammonium chloride, water, and brine and then dried over MgSO₄. The crude product is purified by column chromatography on silica gel, using a mixture of methylene chloride/pentane (60/40) as the eluent to afford an orange oil (800 mg, 67%). ¹H NMR (300 MHz, CDCl₃, ppm): δ 6.80 (d, *J* = 1.0 Hz, 2H), 2.43 (d, *J* = 1 Hz, 6H). ¹³C NMR (75 MHz, CDCl₃, ppm): δ 184.4, 140.72, 139.48, 127.01, 114.85, 15.52. IR (neat): 1611, 1436, 1395, 1230, 1141, 759, 474 cm^{-1} . mp 48 °C. HRMS (EI): calcd 377.8383; found, 377.8382.

Bis(5,5'-dimethyl-[2,2'-bithiophen]-3-yl)methanone (1ss). A mixture of bis(2-bromo-5-methylthiophen-3-yl)methanone (200 mg, 0.526 mmol), tributyl(5-methylthiophen-2-yl)stannane (488 mg, 1.26 mmol), and Pd(PPh₃)₄ (111 mg, 20 mol %) is dissolved in 20 mL of toluene. The solution is degassed for 30 min (Ar) and then refluxed for 15 h under argon. After concentration, the residue is dissolved in CH₂Cl₂ and the organic phase is washed with water. After drying over MgSO₄ and solvent removal, the residue is purified by flash column chromatography on silica gel using a mixture of

pentane/methylene chloride (6/4) as the eluent to afford a yellow oil (160 mg, 73%). Monocrystals are obtained by crystallization in EtOH. ^1H NMR (300 MHz, CDCl_3 , ppm): δ 6.96 (d, $J = 3.6$ Hz, 1H), 6.77 (d, $J = 1.1$ Hz, 1H), 6.59 (dd, $J = 3.6, 0.9$ Hz, 1H), 2.43 (d, $J = 0.9$ Hz, 3H), 2.35 (d, $J = 1.1$ Hz, 3H). ^{13}C NMR (75 MHz, CDCl_3 , ppm): δ 186.6, 141.8, 140.0, 137.4, 137.1, 132.3, 128.4, 128.2, 125.7, 15.4, 15.0. IR (neat): 1627, 1432, 1136, 773, 728, 488 cm^{-1} . mp 66 $^\circ\text{C}$. HRMS: calcd 414.0240; found, 414.0225. X-ray structure: monoclinic, $C2/c$.

General Procedure for the Preparation of Spiro Derivatives from the Corresponding Bis-arylmethanone. The ketone is dispersed in appropriate volume of methanesulfonic acid, and the reaction mixture is stirred overnight. The solution is slowly poured on a large amount of icy water and extracted with methylene chloride. The recombined organic phases are washed with a saturated solution of NaHCO_3 , water, and brine. After drying over MgSO_4 , the solvent is removed. The residue is purified by flash column chromatography on silica gel using a mixture of pentane/methylene chloride (8/2) as the eluent to afford the desired compound.

9,9'-Spiro[fluorene] (spiro-1c). Di([1,1'-biphenyl]-2-yl)-methanone (**1c**) (250 mg, 0.747 mmol), methanesulfonic acid (500 mL), $C = 1.49$ $\text{mmol}\cdot\text{L}^{-1}$, stirred at 120 $^\circ\text{C}$ to obtain the desired compound as a white solid (170 mg, 71%). ^1H NMR (300 MHz, CDCl_3): δ 7.85 (d, 4H, $J = 7.5$ Hz), 7.37 (t, 4H, $J = 7.5$ Hz), 7.11 (t, 4H, $J = 7.5$ Hz), 6.74 (d, 4H, $J = 7.5$ Hz). All physical data were in agreement with those reported in the literature.³⁹

4,4'-Spiro[indeno[1,2-*b*]thiophene] (spiro-1s). Bis(2-(thiophen-2-yl)phenyl)methanone (**1s**) (130 mg, 0.38 mmol), methanesulfonic acid (250 mL), and $C = 1.52$ $\text{mmol}\cdot\text{L}^{-1}$ are stirred at room temperature to obtain the desired compound as a white solid (90 mg, 73%). ^1H NMR (300 MHz, CDCl_3 , ppm): δ 7.53 (d, 2H, $J = 7.5$ Hz), 7.30 (td, 2H, $J = 7.5$ Hz, $J = 1.2$ Hz), 7.23 (d, 2H, $J = 4.8$ Hz), 7.01 (td, 2H, $J = 7.5$ Hz, $J = 1.2$ Hz), 6.72 (d, 2H, $J = 7.5$ Hz), 6.54 (d, 2H, $J = 4.8$ Hz). ^{13}C NMR (75 MHz, CDCl_3 , ppm): δ 150.9, 149.7, 143.6, 138.6, 127.9, 127.8, 125.9, 123.4, 121.3, 118.9, 60.9. IR (neat): 1451, 840, 748, 673, 656 cm^{-1} . mp 168 $^\circ\text{C}$. MS (MALDI-TOF) [M^+]: 328.2. HRMS: calcd 328.0380; found, 328.0372.

4,4'-Spiro[indeno[1,2-*b*]selenophene] (spiro-1se). Bis(2-(selenophen-2-yl)phenyl)methanone (**1se**) (100 mg, 0.22 mmol), methanesulfonic acid (150 mL), and $C = 1.46$ $\text{mmol}\cdot\text{L}^{-1}$ are stirred at room temperature to obtain the desired compound as a white solid (20 mg, 20%). ^1H NMR (300 MHz, CDCl_3 , ppm): δ 7.85 (d, $J = 5.4$ Hz, 2H), 7.51 (dd, $J = 7.5, 0.9$ Hz, 2H), 7.29 (td, $J = 7.6, 1.0$ Hz, 2H), 7.02 (td, $J = 7.5, 1.0$ Hz, 2H), 6.73 (dd, $J = 7.5, 0.9$ Hz, 2H), 6.70 (d, $J = 5.4$ Hz, 2H). ^{13}C NMR (75 MHz, CDCl_3 , ppm): δ 151.6, 148.5, 146.4, 141.2, 132.8, 127.9, 126.0, 123.9, 123.3, 119.7, 63.8. IR (neat): 1475, 809, 750, 729, 665 cm^{-1} . mp 149 $^\circ\text{C}$. HRMS (MALDI-TOF) [M^{\bullet}]: calcd 423.9269; found, 423.9268.

1,1'-Dimethyl-1H,1'H-4,4'-spiro[indeno[1,2-*b*]pyrrole] (spiro-1n). Bis(2-(1-methyl-1H-pyrrol-2-yl)phenyl)-methanone (**1n**) (100 mg, 0.29 mmol), methanesulfonic acid (250 mL), and $C = 1.16$ $\text{mmol}\cdot\text{L}^{-1}$ are stirred at room temperature to obtain the desired compound as a white solid (70 mg, 74%). ^1H NMR (300 MHz, CDCl_3 , ppm): δ 7.38 (d, $J = 7.5$ Hz, 2H), 7.17 (td, $J = 7.5, 1.0$ Hz, 2H), 6.85 (td, $J = 7.5, 1.0$ Hz, 2H), 6.67 (d, $J = 7.5$ Hz, 2H), 6.60 (d, $J = 2.6$ Hz, 2H), 5.74 (d, $J = 2.6$ Hz, 2H), 3.96 (s, 6H). ^{13}C NMR (75 MHz,

CDCl_3 , ppm): δ 153.1, 138.6, 136.1, 133.5, 126.8, 126.5, 124.0, 123.6, 115.8, 102.8, 35.17 (s). IR (neat): 1459, 762, 714 cm^{-1} . mp 150 $^\circ\text{C}$. HRMS (MALDI-TOF): calcd 322.1470; found, 322.1459.

10,10'-Spiro[benzo[*b*]indeno[2,1-*d*]thiophene] (spiro-2s). Bis-(3-(benzo[*b*]thiophen-2-yl)phenyl) methanone (**2s**) (300 mg, 0.67 mmol), methanesulfonic acid (580 mL), are $C = 1.16$ $\text{mmol}\cdot\text{L}^{-1}$ are stirred at room temperature to obtain the desired compound as a white solid (260 mg, 90%). ^1H NMR (300 MHz, CDCl_3 , ppm): δ 7.81 (d, $J = 8.2$ Hz, 2H), 7.70 (d, $J = 7.6$ Hz, 2H), 7.38 (t, $J = 7.1$ Hz, 2H), 7.13 (t, $J = 8.3$ Hz, 2H), 7.07 (t, $J = 7.5$ Hz, 2H), 6.97 (t, $J = 7.6$ Hz, 2H), 6.80 (d, $J = 7.5$ Hz, 2H), 6.65 (d, $J = 8.0$ Hz, 2H). ^{13}C NMR (75 MHz, CDCl_3 , ppm): δ 149.1, 144.2, 114.0, 142.4, 139.2, 133.4, 128.3, 126.9, 124.9, 124.2, 123.7, 123.6, 121.1, 120.1, 61.5. IR (neat): 1448, 744, 727, 716, 443 cm^{-1} . mp 225 $^\circ\text{C}$. MALDI-TOF: 428.0. HRMS (MALDI-TOF): calcd 428.0693; found, 428.0683.

2,2'-Dimethyl-4,4'-spiro[indeno[1,2-*B*]thiophene] (spiro-3s). Bis(2-(5-methylthiophen-2-yl)phenyl) methanone (**3s**) (400 mg, 1.07 mmol), methanesulfonic acid (50 mL), and $C = 21.4$ $\text{mmol}\cdot\text{L}^{-1}$ are stirred at room temperature to obtain the desired compound as a white solid (180 mg, 47%). ^1H NMR (300 MHz, CDCl_3 , ppm): δ 7.45 (d, $J = 7.5$ Hz, 2H), 7.26 (s, 2H), 6.98 (td, $J = 7.5, 1.0$ Hz, 2H), 6.72 (d, $J = 7.5$ Hz, 2H), 6.24 (d, $J = 1.0$ Hz, 2H), 2.46 (d, $J = 0.9$ Hz, 6H). ^{13}C NMR (75 MHz, CDCl_3 , ppm): δ 150.1, 149.0, 143.6, 141.1, 139.3, 127.8, 125.3, 123.3, 119.7, 118.5, 61.6, 16.4. IR (neat): 1456, 748 cm^{-1} . mp 155 $^\circ\text{C}$. MALDI-TOF: 356.4. HRMS (FAB $^+$): calcd 356.0693; found, 356.0695.

4,4'-Spiro[indeno[1,2-*b*]thiophene] (spiro-4s). Bis(2-(thiophen-2-yl)phenyl)methanone (**4s**) (130 mg, 0.38 mmol) and methanesulfonic acid (250 mL) are stirred at room temperature for 12 h to obtain the desired compound as a white solid (90 mg, 73%). ^1H NMR (300 MHz, CDCl_3 , ppm): δ 7.53 (d, 2H, $J = 7.5$ Hz), 7.30 (td, 2H, $J = 7.5$ Hz, $J = 1.2$ Hz), 7.23 (d, 2H, $J = 4.8$ Hz), 7.01 (td, 2H, $J = 7.5$ Hz, $J = 1.2$ Hz), 6.72 (d, 2H, $J = 7.5$ Hz), 6.54 (d, 2H, $J = 4.8$ Hz). ^{13}C NMR (75 MHz, CDCl_3 , ppm): δ 150.9, 149.7, 143.6, 138.6, 127.9, 127.8, 125.9, 123.4, 121.3, 118.9, 60.9. IR (neat): 1451, 840, 748, 673, 656 cm^{-1} . mp 168 $^\circ\text{C}$. MS (MALDI-TOF) [M^+]: 328.2. HRMS (FAB $^+$): calcd 328.0380; found, 328.0372.

Computational Details. All calculations have been performed with the Gaussian 09 program.⁴⁰ For all molecules, the gas-phase ground-state geometries have been optimized, without forcing any symmetry, by a DFT method with the hybrid PBE0 functional (with 25% of exact exchange)⁴¹ and the augmented and polarized Pople double zeta basis set 6-31+G(2d,2p). All ground-state geometries have been verified by frequency calculation showing that the stationary point corresponds to a global minimum on the potential energy surface. To determine the Fukui functions and dual descriptors, the electron densities have been calculated with ($N + 1$) and ($N - 1$) electrons, without changing the geometry (single-point calculations). The condensed Fukui and dual descriptor values were obtained through the Hirshfeld charge difference method (Yang–Mortier scheme).⁴² The Hirshfeld population analysis used takes into account the interatomic electrostatic interactions (named HirshfeldEE in Gaussian).⁴³ Molecular orbitals (MOs), Fukui functions, and dual descriptor (f^+ , f^- , f^{dual}) pictures have been generated by a homemade automated program interfaced with Pov-Ray.⁴⁴

Cutoff values have been automatically set to correspond to an integration of 20% for MO, f^+ and f^- , and 25% for f^{total} .

■ ASSOCIATED CONTENT

● Supporting Information

The Supporting Information is available free of charge on the ACS Publications website at DOI: 10.1021/acsomega.8b03368.

^1H and ^{13}C NMR data, crystallographic data for all ketones, ^1H and ^{13}C NMR data for all spiro derivatives, and computational data of protonated ketones (PDF)

■ AUTHOR INFORMATION

Corresponding Authors

*E-mail: lionel.sanguinet@univ-angers.fr (L.S.).

*E-mail: philippe.leriche@univ-angers.fr (P.L.).

ORCID

Lionel Sanguinet: 0000-0002-4334-9937

Thomas Cauchy: 0000-0003-4259-3257

Notes

The authors declare no competing financial interest.

■ ACKNOWLEDGMENTS

C.D. and V.J. thank the University of Angers for granting. The authors thank the Johnson Matthey Company for their generous providing of palladium salts. P.L. and L.S. are grateful to Dr Clément Cabanetos for fruitful and heady discussions. The authors thank B. Siegler and Dr I. Freuze for their assistance in NMR spectroscopy and MS, respectively.

■ REFERENCES

(1) Kanibolotsky, A. L.; Perepichka, I. F.; Skabara, P. J. Star-shaped π -conjugated oligomers and their applications in organic electronics and photonics. *Chem. Soc. Rev.* **2010**, *39*, 2695–2728.

(2) (a) Ponomarenko, S. A.; Luponosov, Y. N.; Min, J.; Solodukhin, A. N.; Surin, N. M.; Shcherbina, M. A.; Chvalun, S. N.; Ameri, T.; Brabec, C. Design of donor-acceptor star-shaped oligomers for efficient solution-processible organic photovoltaics. *Faraday Discuss.* **2014**, *174*, 313–339. (b) Roncali, J.; Leriche, P.; Cravino, A. From One- to Three-Dimensional Organic Semiconductors: In Search of the Organic Silicon? *Adv. Mater.* **2007**, *19*, 2045–2060.

(3) Chan, C.-Y.; Wong, Y.-C.; Wong, H.-L.; Chan, M.-Y.; Wing-Wah Yam, V. A new class of three-dimensional, p-type, spirobifluorene-modified perylene diimide derivatives for small molecular-based bulk heterojunction organic photovoltaic devices. *J. Mater. Chem. C* **2014**, *2*, 7656–7665.

(4) (a) Luo, J.; Zhou, Y.; Niu, Z.-Q.; Zhou, Q.-F.; Ma, Y.; Pei, J. Three-Dimensional Architectures for Highly Stable Pure Blue Emission. *J. Am. Chem. Soc.* **2007**, *129*, 11314–11315. (b) Saragi, T. P. I.; Spehr, T.; Siebert, A.; Fuhrmann-Lieker, T.; Salbeck, J. Spiro compounds for organic optoelectronics. *Chem. Rev.* **2007**, *107*, 1011–1065. (c) Cocherel, N.; Poriel, C.; Rault-Berthelot, J.; Barrière, F.; Audebrand, N.; Slawin, A. M. Z.; Vignau, L. New 3 π -2Spiro Ladder-Type Phenylene Materials: Synthesis, Physicochemical Properties and Applications in OLEDs. *Chem.—Eur. J.* **2008**, *14*, 11328–11342. (d) Cho, Y. J.; Lee, J. Y. Thermally stable aromatic amine derivative with symmetrically substituted double spirobifluorene core as a hole transport material for green phosphorescent organic light-emitting diodes. *Thin Solid Films* **2012**, *522*, 415–419. (e) Thirion, D.; Poriel, C.; Métivier, R.; Rault-Berthelot, J.; Barrière, F.; Jeannin, O. Violet-to-Blue Tunable Emission of Aryl-Substituted Dispirofluorene-Indenofluorene Isomers by Conformationally-Controllable Intramolecular Excimer Formation. *Chem.—Eur. J.* **2011**, *17*, 10272–10287.

(5) (a) Thiery, S.; Tondelier, D.; Declairieux, C.; Seo, G.; Geffroy, B.; Jeannin, O.; Rault-Berthelot, J.; Métivier, R.; Poriel, C. 9,9'-Spirobifluorene and 4-phenyl-9,9'-spirobifluorene: pure hydrocarbon small molecules as hosts for efficient green and blue PhOLEDs. *J. Mater. Chem. C* **2014**, *2*, 4156–4166. (b) Kwon, Y. S.; Lim, J.; Yun, H.-J.; Kim, Y.-H.; Park, T. A diketopyrrolopyrrole-containing hole transporting conjugated polymer for use in efficient stable organic-inorganic hybrid solar cells based on a perovskite. *Energy Environ. Sci.* **2014**, *7*, 1454–1460. (c) Wang, M.; Li, C.; Lv, A.; Wang, Z.; Bo, Z. Spirobifluorene-Based Conjugated Polymers for Polymer Solar Cells with High Open-Circuit Voltage. *Macromolecules* **2012**, *45*, 3017–3022. (d) Macor, L.; Gervaldo, M.; Fungo, F.; Otero, L.; Ditttrich, T.; Lin, C.-Y.; Chi, L.-C.; Fang, F.-C.; Lii, S.-W.; Wong, K.-T.; Tsai, C.-H.; Wu, C.-C. Photoinduced charge separation in donor-acceptor spiro compounds at metal and metal oxide surfaces: application in dye-sensitized solar cell. *RSC Adv.* **2012**, *2*, 4869–4878. (e) Ma, S.; Fu, Y.; Ni, D.; Mao, J.; Xie, Z.; Tu, G. Spiro-fluorene based 3D donor towards efficient organic photovoltaics. *Chem. Commun.* **2012**, *48*, 11847–11849. (f) Wang, J.; Dai, S.; Yao, Y.; Cheng, P.; Lin, Y.; Zhan, X. Spirobifluorene-based acceptors for polymer solar cells: Effect of isomers. *Dyes Pigm.* **2015**, *123*, 16–25.

(6) Economopoulos, S. P.; Itskos, G.; Koutentis, P. A.; Choulis, S. A. Overview of Polymer and Copolymer Materials for Organic Photovoltaics. In *Organic Photovoltaics*; Wiley-VCH Verlag GmbH & Co. KGaA, 2014; pp 1–26.

(7) Sharma, A.; Pathak, D.; Wagner, T. Organic photovoltaic materials: a review on synthesis, structure and properties. *J. Optoelectron. Adv. Mater.* **2014**, *16*, 1257–1268.

(8) (a) Ko, S.; Choi, H.; Kang, M.-S.; Hwang, H.; Ji, H.; Kim, J.; Ko, J.; Kang, Y. Silole-spaced triarylamine derivatives as highly efficient organic sensitizers in dye-sensitized solar cells (DSSCs). *J. Mater. Chem.* **2010**, *20*, 2391–2399. (b) Baheti, A.; Justin Thomas, K. R.; Li, C.-T.; Lee, C.-P.; Ho, K.-C. Fluorene-Based Sensitizers with a Phenothiazine Donor: Effect of Mode of Donor Tethering on the Performance of Dye-Sensitized Solar Cells. *ACS Appl. Mater. Interfaces* **2015**, *7*, 2249–2262. (c) Baheti, A.; Gajjela, S. R.; Balaya, P.; Justin Thomas, K. R. Synthesis, optical, electrochemical and photovoltaic properties of organic dyes containing trifluorenylamine donors. *Dyes Pigm.* **2015**, *113*, 78–86. (d) Baheti, A.; Justin Thomas, K. R.; Lin, L.-C.; Lee, K.-M. Monoanchoring (D-D- π -A) and Dianchoring (D-D-(π -A) $_2$) Organic Dyes Featuring Triarylamine Donors Composed of Fluorene and Carbazole. *Asian J. Org. Chem.* **2014**, *3*, 886–898. (e) Baheti, A.; Justin Thomas, K. R.; Lee, C.-P.; Li, C.-T.; Ho, K.-C. Organic dyes containing fluorene-9-ylidene chromophores for efficient dye-sensitized solar cells. *J. Mater. Chem. A* **2014**, *2*, 5766–5779. (f) Thomas, K. R. J.; Baheti, A. Fluorene based organic dyes for dye sensitised solar cells: structure-property relationships. *Mater. Technol.* **2013**, *28*, 71–87. (g) Baheti, A.; Thomas, K. R. J.; Lee, C.-P.; Ho, K.-C. Synthesis and characterization of dianchoring organic dyes containing 2,7-diaminofluorene donors as efficient sensitizers for dye-sensitized solar cells. *Org. Electron.* **2013**, *14*, 3267–3276. (h) Singh, P.; Baheti, A.; Thomas, K. R. J.; Lee, C.-P.; Ho, K.-C. Fluorene-based organic dyes containing acetylene linkage for dye-sensitized solar cells. *Dyes Pigm.* **2012**, *95*, 523–533. (i) Baheti, A.; Thomas, K. R. J.; Ng, S. W.; Tiekink, E. R. T. N-(7-Bromo-9-butyl-9H-carbazol-2-yl)-9,9-diethyl-N,N,N-triphenyl-9H-fluorene-2,7-diamine. *Acta Crystallogr., Sect. E: Struct. Rep. Online* **2012**, *68*, o860–o861. (j) Baheti, A.; Thomas, K. R. J.; Lee, C.-P.; Ho, K.-C. Fine Tuning the Performance of DSSCs by Variation of the π -Spacers in Organic Dyes that Contain a 2,7-Diaminofluorene Donor. *Chem.—Asian J.* **2012**, *7*, 2942–2954. (k) Thomas, K. R. J.; Singh, P.; Baheti, A.; Hsu, Y.-C.; Ho, K.-C.; Lin, J. T. s. Electro-optical properties of new anthracene based organic dyes for dye-sensitized solar cells. *Dyes Pigm.* **2011**, *91*, 33–43. (l) Baheti, A.; Singh, P.; Justin Thomas, K. R. The synthesis and spectral characterization of red dyes containing biphenyl or fluorene conjugation and dicyanovinyl acceptors. *Dyes Pigm.* **2011**, *88*, 195–203. (m) Baheti, A.; Singh, P.; Lee, C.-P.; Thomas, K. R. J.; Ho, K.-C. 2,7-Diaminofluorene-Based Organic Dyes for Dye-Sensitized Solar Cells: Effect of Auxiliary Donor on Optical

- and Electrochemical Properties. *J. Org. Chem.* **2011**, *76*, 4910–4920.
- (n) Baheti, A.; Lee, C.-P.; Thomas, K. R. J.; Ho, K.-C. Pyrene-based organic dyes with thiophene containing π -linkers for dye-sensitized solar cells: optical, electrochemical and theoretical investigations. *Phys. Chem. Chem. Phys.* **2011**, *13*, 17210–17221.
- (o) Baheti, A.; Tyagi, P.; Thomas, K. R. J.; Hsu, Y.-C.; Lin, J. T. Simple Triarylamine-Based Dyes Containing Fluorene and Biphenyl Linkers for Efficient Dye-Sensitized Solar Cells. *J. Phys. Chem. C* **2009**, *113*, 8541–8547.
- (9) Koumura, N.; Hara, K. Development of Carbazole Dyes For efficient Molecular Photovoltaics. *Heterocycles* **2013**, *87*, 275–301.
- (10) (a) Li, G.; Kang, C.; Gong, X.; Zhang, J.; Li, C.; Chen, Y.; Dong, H.; Hu, W.; Li, F.; Bo, Z. 5-Alkyloxy-6-fluorobenzo[c][1,2,5]-thiadiazole- and Silafluorene-Based D-A Alternating Conjugated Polymers: Synthesis and Application in Polymer Photovoltaic Cells. *Macromolecules* **2014**, *47*, 4645–4652. (b) Yuan, M.; Yang, P.; Durban, M. M.; Luscombe, C. K. Low Bandgap Polymers Based on Silafluorene Containing Multifused Heptacyclic Arenes for Photovoltaic Applications. *Macromolecules* **2012**, *45*, 5934–5940.
- (11) Jäger, M.; Trattning, R.; Postl, M.; Haas, W.; Kunert, B.; Resel, R.; Hofer, F.; Klug, A.; Trimmel, G.; List, E. J. W. Influence of the bridging atom in fluorene analogue low-bandgap polymers on photophysical and morphological properties of copper indium sulfide/polymer nanocomposite solar cells. *J. Polym. Sci., Part B: Polym. Phys.* **2013**, *51*, 1400.
- (12) (a) Tang, W.; Huang, D.; He, C.; Yi, Y.; Zhang, J.; Di, C.; Zhang, Z.; Li, Y. Solution-processed small molecules based on indacenodithiophene for high performance thin-film transistors and organic solar cells. *Org. Electron.* **2014**, *15*, 1155–1165. (b) Lin, Y.; Zhan, X. Oligomer Molecules for Efficient Organic Photovoltaics. *Acc. Chem. Res.* **2016**, *49*, 175–183.
- (13) Yen, Y.-S.; Chen, W.-T.; Hsu, C.-Y.; Chou, H.-H.; Lin, J. T.; Yeh, M.-C. P. Arylamine-Based Dyes for p-Type Dye-Sensitized Solar Cells. *Org. Lett.* **2011**, *13*, 4930–4933.
- (14) Clarkson, R. G.; Gomberg, M. Spirans with Four Aromatic Radicals on the Spiro Carbon Atom. *J. Am. Chem. Soc.* **1930**, *52*, 2881–2891.
- (15) Wynberg, H.; Heeres, G. J.; Jordens, P.; Sinnige, H. J. M. The synthesis and spectra of some heterocyclic conjugated spiranes. *Recl. Trav. Chim. Pays-Bas* **1970**, *89*, 545–552.
- (16) Mitschke, U.; Bäuerle, P. Synthesis, characterization, and electrogenerated chemiluminescence of phenyl-substituted, phenyl-annulated, and spirofluorenyl-bridged oligothiophenes. *J. Chem. Soc., Perkin Trans. 1* **2001**, 740–753.
- (17) Ong, T.-T.; Ng, S.-C.; Chan, H. S. O.; Vardhanan, R. V.; Kumura, K.; Mazaki, Y.; Kobayashi, K. Development of a novel isotype organic heterojunction diode consisting of poly{7-spiro(9-fluorenyl)cyclopentadithiophene} and poly(3-octylthiophene). *J. Mater. Chem.* **2003**, *13*, 2185–2188.
- (18) Ting, H.-C.; Tsai, C.-H.; Chen, J.-H.; Lin, L.-Y.; Chou, S.-H.; Wong, K.-T.; Huang, T.-W.; Wu, C.-C. A Novel Amine-Free Dianchoring Organic Dye for Efficient Dye-Sensitized Solar Cells. *Org. Lett.* **2012**, *14*, 6338–6341.
- (19) Pozzi, G.; Orlandi, S.; Cavazzini, M.; Minudri, D.; Macor, L.; Otero, L.; Fungo, F. Synthesis and Photovoltaic Applications of a 4,4'-Spirobi[cyclopenta[2,1-b;3,4-b']dithiophene]-Bridged Donor/Acceptor Dye. *Org. Lett.* **2013**, *15*, 4642–4645.
- (20) Jeux, V.; Dalinot, C.; Allain, M.; Sanguinet, L.; Leriche, P. Synthesis of Spiro[cyclopenta[1,2-b;5,4-b']DiThiophene-4,9'-Fluorenes] SDTF dissymmetrically functionalized. *Tetrahedron Lett.* **2015**, *56*, 1383–1387.
- (21) (a) Cheng, X.; Zhu, S.-F.; Qiao, X.-C.; Yan, P.-C.; Zhou, Q.-L. A general synthetic route to chiral dihydroxy-9,9'-spirobifluorenes. *Tetrahedron* **2006**, *62*, 8077–8082. (b) Cheng, X.; Hou, G.-H.; Xie, J.-H.; Zhou, Q.-L. Synthesis and Optical Resolution of 9,9'-Spirobifluorene-1,1'-diol. *Org. Lett.* **2004**, *6*, 2381–2383.
- (22) Chiang, C.-L.; Shu, C.-F.; Chen, C.-T. Improved Synthesis of 2,2'-Dibromo-9,9'-spirobifluorene and Its 2,2'-Bisdonor-7,7'-bisacceptor-Substituted Fluorescent Derivatives. *Org. Lett.* **2005**, *7*, 3717–3720.
- (23) Hirao, H.; Ohwada, T. Theoretical Study of Reactivities in Electrophilic Aromatic Substitution Reactions: Reactive Hybrid Orbital Analysis. *J. Phys. Chem. A* **2003**, *107*, 2875–2881.
- (24) Fukui, K.; Yonezawa, T.; Shingu, H. A Molecular Orbital Theory of Reactivity in Aromatic Hydrocarbons. *J. Chem. Phys.* **1952**, *20*, 722–725.
- (25) (a) Parr, R. G.; Weitao, Y. *Density-Functional Theory of Atoms and Molecules*; Oxford University Press, 1994; (b) Geerlings, P.; De Proft, F.; Langenaeker, W. Conceptual Density Functional Theory. *Chem. Rev.* **2003**, *103*, 1793–1874. (c) Chermette, H. Chemical reactivity indexes in density functional theory. *J. Comput. Chem.* **1999**, *20*, 129–154. (d) Chattaraj, P. K.; Sarkar, U.; Roy, D. R. Electrophilicity Index. *Chem. Rev.* **2006**, *106*, 2065–2091. (e) Chattaraj, P. K. *Chemical Reactivity Theory: A Density Functional View*; CRC Press/Taylor & Francis: Boca Raton, 2009; (f) Toro-Labbé, A. *Theoretical Aspects of Chemical Reactivity*, 1st ed.; Elsevier: Amsterdam, Boston, 2007.
- (26) (a) Yamamoto, A.; Ohta, E.; Kishigami, N.; Tsukahara, N.; Tomiyori, Y.; Sato, H.; Matsui, Y.; Kano, Y.; Mizuno, K.; Ikeda, H. Synthesis and basic properties of tetrathieno[2,3-a:3',2'-c:2'',3''-f:3''',2''''-h]naphthalene: a new π -conjugated system obtained by photoinduced electro-dehydrogenation reactions of tetra(3-thienyl)-ethene. *Tetrahedron Lett.* **2013**, *54*, 4049–4053. (b) Neumann, H.; Brennfürer, A.; Beller, M. A general synthesis of diarylketones by means of a three-component cross-coupling of Aryl and heteroaryl bromides, carbon monoxide, and boronic acids. *Chem.—Eur. J.* **2008**, *14*, 3645–3652. (c) Martyres, D.; Schmiedt, F. A short synthesis of 3,3-di(hetero)arylpropylamines obtained from bis-(hetero)aryl ketones via palladium catalysis. *Tetrahedron Lett.* **2006**, *47*, 1649–1651. (d) Enquist, P.-A.; Nilsson, P.; Larhed, M. Ultrafast Chemistry: Cobalt Carbonyl-Mediated Synthesis of Diaryl Ketones under Microwave Irradiation. *Org. Lett.* **2003**, *5*, 4875–4878. (e) Lucas, P.; Mehdi, N. E.; Ho, H. A.; Bélanger, D.; Breaux, L. Expedient synthesis of symmetric aryl ketones and of ambient-temperature molten salts of imidazole. *Synthesis* **2000**, 1253–1258. (f) Strekowski, L.; Wydra, R. L.; Cegla, M. T.; Czarny, A.; Patterson, S. Efficient preparation of ketones from N-(ethoxymethylene)aniline and organometallic reagents. *J. Org. Chem.* **1989**, *54*, 6120–6123.
- (27) Clarkson, R. G.; Gomberg, M. Spirans with Four Aromatic Radicals on the Spiro Carbon Atom. *J. Am. Chem. Soc.* **1930**, *52*, 2881–2891.
- (28) Sargent, M. V.; Dean, F. M. 3.11—Furans and Their Benzo Derivatives: (ii) Reactivity A2. In *Comprehensive Heterocyclic Chemistry*; Katritzky, A. R., Rees, C. W., Ed.; Pergamon: Oxford, 1984; pp 599–656.
- (29) Chapter 6 Reactivity of Five-Membered Rings Containing one Heteroatom. In *Advances in Heterocyclic Chemistry*; Katritzky, A. R., Taylor, R. W., Ed.; Academic Press, 1990; Vol. 47, pp 87–137.
- (30) Langenaeker, W.; Demel, K.; Geerlings, P. Quantum-chemical study of the Fukui function as a reactivity index. *J. Mol. Struct.: THEOCHEM* **1991**, *234*, 329–342.
- (31) Echeagaray, E.; Cárdenas, C.; Rabi, S.; Rabi, N.; Lee, S.; Zadeh, F. H.; Toro-Labbé, A.; Anderson, J. S. M.; Ayers, P. W. In pursuit of negative Fukui functions: examples where the highest occupied molecular orbital fails to dominate the chemical reactivity. *J. Mol. Model.* **2013**, *19*, 2779–2783.
- (32) (a) Moriishi, H.; Kikuchi, O.; Suzuki, K.; Klopman, G. Reaction potential map analysis of chemical reactivity?III. *Theor. Chim. Acta* **1984**, *64*, 319–338. (b) Tasi, G.; Palinko, I.; Nyerges, L.; Fejes, P.; Foerster, H. Calculation of electrostatic potential maps and atomic charges for large molecules. *J. Chem. Inf. Comput. Sci.* **1993**, *33*, 296–299.
- (33) Chattaraj, P. K. Chemical Reactivity and Selectivity: Local HSAB Principle versus Frontier Orbital Theory. *J. Phys. Chem. A* **2001**, *105*, 511–513.
- (34) Morell, C.; Grand, A.; Toro-Labbé, A. New Dual Descriptor for Chemical Reactivity. *J. Phys. Chem. A* **2005**, *109*, 205–212.
- (35) Anderson, J. S. M.; Melin, J.; Ayers, P. W. Conceptual Density-Functional Theory for General Chemical Reactions, Including Those

That Are Neither Charge- nor Frontier-Orbital-Controlled. 1. Theory and Derivation of a General-Purpose Reactivity Indicator. *J. Chem. Theory Comput.* **2007**, *3*, 358–374.

(36) Berkowitz, M. Density functional approach to frontier controlled reactions. *J. Am. Chem. Soc.* **1987**, *109*, 4823–4825.

(37) Fleming, I. Chemical Reactions—How Far and How Fast. *Molecular Orbitals and Organic Chemical Reactions*; John Wiley & Sons, Ltd, 2010; pp 127–144.

(38) Coulson, D. R.; Satek, L. C.; Grim, S. O. Tetrakis-(triphenylphosphine)palladium(0). *Inorganic Syntheses*; John Wiley & Sons, Inc., 2007; pp 121–124.

(39) Ren, L.; Jiao, N. Pd/Cu-Cocatalyzed Aerobic Oxidative Carbonylative Homocoupling of Arylboronic Acids and CO: A Highly Selective Approach to Diaryl Ketones. *Chem.—Asian J.* **2014**, *9*, 2411–2414.

(40) Frisch, M. J.; Trucks, G. W.; Schlegel, H. B.; Scuseria, G. E.; Robb, M. A.; Cheeseman, J. R.; Scalmani, G.; Barone, V.; Mennucci, B.; Petersson, G. A.; Nakatsuji, H.; Caricato, M.; Li, X.; Hratchian, H. P.; Izmaylov, A. F.; Bloino, J.; Zheng, G.; Sonnenberg, J. L.; Hada, M.; Ehara, M.; Toyota, K.; Fukuda, R.; Hasegawa, J.; Ishida, M.; Nakajima, T.; Honda, Y.; Kitao, O.; Nakai, H.; Vreven, T.; Montgomery, J. A., Jr.; Peralta, J. E.; Ogliaro, F.; Bearpark, M.; Heyd, J. J.; Brothers, E.; Kudin, K. N.; Staroverov, V. N.; Kobayashi, R.; Normand, J.; Raghavachari, K.; Rendell, A.; Burant, J. C.; Iyengar, S. S.; Tomasi, J.; Cossi, M.; Rega, N.; Millam, J. M.; Klene, M.; Knox, J. E.; Cross, J. B.; Bakken, V.; Adamo, C.; Jaramillo, J.; Gomperts, R.; Stratmann, R. E.; Yazyev, O.; Austin, A. J.; Cammi, R.; Pomelli, C.; Ochterski, J. W.; Martin, R. L.; Morokuma, K.; Zakrzewski, V. G.; Voth, G. A.; Salvador, P.; Dannenberg, J. J.; Dapprich, S.; Daniels, A. D.; Farkas, Ö.; Foresman, J. B.; Ortiz, J. V.; Cioslowski, J.; Fox, D. J. *Gaussian 09*, Revision D.01; Gaussian Inc, 2009.

(41) (a) Perdew, J. P.; Burke, K.; Ernzerhof, M. Generalized gradient approximation made simple. *Phys. Rev. Lett.* **1996**, *77*, 3865–3868.

(b) Adamo, C.; Barone, V. Toward reliable density functional methods without adjustable parameters: The PBE0 model. *J. Chem. Phys.* **1999**, *110*, 6158–6170.

(42) (a) Parr, R. G.; Yang, W. Density functional approach to the frontier-electron theory of chemical reactivity. *J. Am. Chem. Soc.* **1984**, *106*, 4049–4050. (b) Yang, W.; Mortier, W. J. The use of global and local molecular parameters for the analysis of the gas-phase basicity of amines. *J. Am. Chem. Soc.* **1986**, *108*, 5708–5711.

(43) (a) Hirshfeld, F. L. Bonded-atom fragments for describing molecular charge densities. *Theor. Chim. Acta* **1977**, *44*, 129–138.

(b) Ritchie, J. P.; Bachrach, S. M. Some methods and applications of electron density distribution analysis. *J. Comput. Chem.* **1987**, *8*, 499–509.

(44) Morille, Y.; Cauchy, T. *ABSiCC Automating Boring Stuff in Computational Chemistry*; University of Angers, 2014.